Journal of Power Sources 195 (2010) 7380–7385

Contents lists available at ScienceDirect

Journal of Power Sources

journal homepage: www.elsevier.com/locate/jpowsour

Improving solid-state hydriding and dehydriding properties of the $LiBH_4$ plus MgH_2 system with the addition of Mn and V dopants

Kyle Crosby, Xuefei Wan, Leon L. Shaw*

Department of Chemical, Materials and Biomolecular Engineering, University of Connecticut, 97 North Eagleville Road, U-3136, Storrs, CT 06269, USA

ARTICLE INFO

Article history:
Received 30 April 2010
Received in revised form 25 May 2010
Accepted 26 May 2010
Available online 31 May 2010

Keywords:
Hydrogen storage materials
Lithium borohydride
Lithium hydride
Transition metal doping

ABSTRACT

The hydriding process of the $2LiH + MgB_2$ mixture is controlled by outward diffusion of Mg and inward diffusion of Li and H within MgB_2 crystals to form $LiBH_4$. This study explores the feasibility of using transition metal dopants, such as Mn and V, to enhance the diffusion rate and thus the hydriding kinetics. It is found that Mn can indeed enhance the hydriding kinetics of the $2LiH + MgB_2$ mixture, while V does not. The major factor in enhancing the diffusion rate and thus the hydriding kinetics is related to the dopant's ability to induce the lattice distortion of MgB_2 crystals. This study demonstrates that the kinetics of the diffusion controlled solid-state hydriding process can be improved by doping if the dopant is properly selected.

1. Introduction

Renewable hydrogen fuel sources are of considerable importance in the wake of present global energy shortages. While advances have been made in the application of compressed gas and liquid state hydrogen storage for mobile applications, solid-state reversible hydrogen storage possesses the potential to surpass the gaseous and liquid state storage in both volumetric and gravimetric storage capacities. Lithium borohydride ($LiBH_4$) is one of the solid-state storage materials that have generated great interest because of its high gravimetric hydrogen density (18.5 wt.% H_2) at room temperature [1–3]. However, $LiBH_4$ has a high chemical stability [3–14]. As a result, temperatures as high as 400 °C are often required to release most of the hydrogen stored in $LiBH_4$. Material advances aimed at decreasing the chemical stability and/or increasing reaction kinetics of $LiBH_4$ are currently pursued by (i) addition of novel catalysts [3,4,9], (ii) nanoengineering to confine $LiBH_4$ in mesoporous scaffolds or mix $LiBH_4$ with nano-tubes and mesoporous gels [10–13], (iii) thermodynamic destabilization of $LiBH_4$ via the partial substitution of Li^+ cations by other cations with larger electronegativites [15–20], and (iv) using additives to stabilize the dehydrogenated state [5–8,21–28]. Addition of MgH_2, as an example of approach (iv), represents a material approach being technologically important as well as scientifically interesting because this approach has reduced the hydrogenation and dehydrogenation temperatures to near 350 °C with the following reversible reaction [7]

$$LiBH_4 + (1/2)MgH_2 = LiH + (1/2)MgB_2 + 2H_2 \quad (1)$$

Recently, it has been shown that solid-state hydriding and dehydriding via Eq. (1) is possible [29]. Through long-time ball milling of $2LiH + MgB_2$ mixtures, 8.3 wt.% hydrogen uptake at 265 °C has been demonstrated, whereas the maximum theoretical uptake for the mixture is 11.4 wt.%. Hydrogen release, although slower than uptake, can also be attained in the solid state (e.g., 2.0 wt.% H_2 at 265 °C). Furthermore, it is found that both solid-state hydriding and dehydriding are diffusion controlled [29]. With the aid of nuclear magnetic resonance (NMR), it is found that long-time ball milling has led to the partial exchange of the Mg^{2+} ions in the MgB_2 crystal by the Li^+ ions from the LiH crystal [30,31]. This partial ion exchange results in the formation of a compound with a composition of $(Mg_{1-x}Li_{2x})B_2$ where x is a variable changing from 0 to less than 1. It is the formation of this intermediate compound $(Mg_{1-x}Li_{2x})B_2$ that greatly enhance the subsequent hydriding reaction because the reaction pathway to form $LiBH_4$ and MgH_2 in the solid state is through the following two elementary reactions [32].

$$2LiH + MgB_2 \rightarrow (Mg_{1-x}Li_{2x})B_2 + xMgH_2 + (2-2x)LiH \quad (2)$$

$$(Mg_{1-x}Li_{2x})B_2 + (2-2x)LiH + 4H_2 \rightarrow 2LiBH_4 + MgH_2 \quad (3)$$

As shown in Eq. (2), the first step in the solid-state hydriding is the ion exchange between Mg and Li ions within MgB_2 to form an intermediate compound $(Mg_{1-x}Li_{2x})B_2$, and MgH_2. This reaction can take place during ball milling [30,31]. As a result, the hydriding reaction can be enhanced by long-time ball milling. The

* Corresponding author. Tel.: +1 860 486 2592; fax: +1 860 486 4745.
E-mail address: Leon.Shaw@Uconn.Edu (L.L. Shaw).

0378-7753/$ – see front matter © 2010 Elsevier B.V. All rights reserved.
doi:10.1016/j.jpowsour.2010.05.052

second step in the solid-state hydriding is the continuous Mg–Li ion exchange and simultaneous hydrogenation of the intermediate compound $(Mg_{1-x}Li_{2x})B_2$, to form the final product $LiBH_4$ – a compound that does not contain any Mg ions [32]. The Mg ions rejected from $(Mg_{1-x}Li_{2x})B_2$ react with H to form crystalline MgH_2. These prior studies [29–32] reveal unambiguously that hydriding of the $LiH + MgB_2$ mixture is controlled by diffusion and the major diffusing species are Mg, Li and H ions. Therefore, the potential approaches to enhance the solid-state hydriding of this promising hydrogen storage material system are (i) nanoengineering to minimize the diffusion distance, (ii) mechanical activation to introduce lattice defects and thus increase the diffusion coefficient, and (iii) doping to increase the vacancy concentration and lattice distortion and thus the diffusion rate.

In this study, the approach of adding dopants to increase the diffusion rate is investigated. Mn and V dopants have been chosen for several reasons. First, MnH and VH are thermodynamically less stable than MgH_2 [33]. Thus, dissolution of Mn and V in MgH_2, if taking place, will lead to thermodynamic destabilization of MgH_2 and possible reduction in the decomposition temperature of MgH_2. Second, Mn has a reasonable solubility in Mg (~0.5 wt.% at room temperature) whereas the solubility of V in Mg is negligible [34]. Since no data of the solubilities of Mn and V in MgB_2 are available, the solubilities of Mn and V in Mg are taken as indicators of the possible difference in the solubility properties. Finally, a recent *ab initio* density functional theory calculation [35] reveals that Mn has the potential to enhance the diffusion rate of Mg vacancies in MgB_2, whereas V does not. The favorable effect of Mn is due to its large atomic radius that induces the lattice distortion of MgB_2, thereby decreasing the migration barrier and increasing the diffusion rate of Mg vacancies. In contrast, the atomic radius of V is closer to that of Mg. As a result, V exerts little or no influence on the diffusion rate of Mg vacancies in MgB_2 [35]. The present study is motivated by this theoretical prediction, and the findings from this study are reported below.

2. Experimental

LiH (95% purity), MgB_2 (~98% purity), Mn (99.95% purity), and V (100% purity) were purchased from Alfa Aesar and used as received. The LiH and MgB_2 particles were sub-micrometers, whereas the Mn and V particles were micrometers in the as-received condition. All materials handling and sample preparation was done in an argon-filled glovebox to prevent H_2O and O_2 contamination. Ball milling was performed under argon atmosphere using a modified Szegvari attritor that is effective in producing a highly uniform product while preventing the formation of a dead zone in the milling product [36]. The canister of the attritor with an inner volume of 700 ml and the balls (6.4 mm in diameter) were made of a stainless steel. The $LiH + MgB_2$ mixtures of ~10 g per batch were prepared using a 2:1 molar ratio according to Eq. (1). For the cases with the manganese and vanadium addition, the same 2:1 molar ratio of $LiH + MgB_2$ was utilized, but in each case 5 mol% of the additive was applied. The ball-to-powder weight ratio was 60:1, the milling speed was 600 rpm, the milling atmosphere was argon of 99.999% purity, and the milling temperature was maintained at 20 °C, achieved by water cooling at a flowing rate of 770 ml min^{-1}. Ball milling time was 3, 24, or 120 h, depending on the specific experiment.

Hydriding and subsequent dehydriding of the $LiH + MgB_2$ mixture were carried out using a commercial Sieverts'-type pressure-composition-temperature (PCT) unit (Advanced Materials Corporation, PA). For hydrogenation, the ball-milled $LiH + MgB_2$ mixture of ~600 mg was loaded into the pressure cell of the PCT unit in a glovebox filled with Ar of 99.999% purity. The loaded pressure cell was evacuated to 10^{-3} bar at room temperature before back filled with H_2 of 99.99% purity at 90 bar. The temperature of the cell was then increased from ambient to 265 °C at a rate of 2 °C min^{-1} and maintained at that temperature for 5 h. For dehydrogenation, the hydrogenated powder described above was first cooled down to room temperature, and then the pressure cell was evacuated to 10^{-3} bar before heating to and holding at 265 °C with the same heating rate and holding time as those in the hydrogenation treatment. The hydrogen pressure in the sample cell was maintained at approximately 0.01 bar during the dehydrogenation holding at 265 °C by evacuating the cell in every 30 min of holding.

The $2LiH + MgB_2$ mixtures before and after ball milling, dehydrogenation and re-hydrogenation were analyzed using a D8 ADVANCE X-ray diffractometer. The operation conditions for the X-ray diffraction (XRD) data collection were Cu K_α radiation, 40 kV, 40 mA, 0.005° min^{-1}, and 0.01° per step. To prevent oxidation during XRD data collection, the sample was sealed in a capillary quartz tube of 1.5 mm in diameter and the loading of the sample to the tube was performed in a glovebox filled with argon. The wall of the capillary quartz tube is 0.01 mm in thickness and thus transparent to the X-ray. To detect any peak shifting of LiH and MgB_2 induced by ball milling and the subsequent hydriding treatment, ~15 wt.% coarse-grained Si of 99.9% purity was added as the internal standard to each sample. The use of the Si within the capillary tube as the internal standard not only provided the reference position, but also avoided the possible effect of the curved front of the powder compact caused by the capillary tube on the peak positions of all the compounds in the powder mixture. In analyzing XRD patterns, the "Peakfit" software was used to fit a XRD peak with the assumption of the line profile being a Lorentzian function. The fitting process was stopped when the R^2 value was larger than 0.95 for the ball milled powders and larger than 0.98 for the un-milled powders. The peak position was then determined from the fitted curve. The typical standard deviation for our peak fit was ±0.0036°.

In addition to monitoring the peak shifting and new phase formation, XRD was also used to estimate the crystallite sizes of LiH and MgB_2 and the lattice microstrain of MgB_2 crystals. The LiH (2 0 0) and MgB_2 (1 0 1) reflections with the diffraction angles at 44.35° and 42.41° are used to estimate their crystallite sizes using the Scherrer formula [37], respectively. The lattice microstrain within MgB_2 was estimated using the (1 1 0) reflection of MgB_2 at the diffraction angle of 59.89° with the aid of the Stokes and Wilson formula [38]. The correction for instrumental broadening was conducted using the procedure described in [39] with the aid of ~15 wt.% coarse-grained silicon (Si) of 99.9% purity as the internal standard in each sample. Note that low-angle reflections (e.g., MgB_2 (1 0 1) peak) were used to estimate the crystallite size, whereas high angle reflections (such as MgB_2 (1 1 0) peak) were utilized to determine the lattice microstrain. This was done in order to minimize the error introduced by neglecting the interplay between broadenings due to the lattice microstrain and nanograins. This procedure is justified by the fact that the XRD broadening approaches pure grain size broadening at low 2θ angles, and approximates to pure lattice microstrain broadening at large 2θ angles [38,39]. Recently, a detailed XRD analysis [40] using the Rietveld method in conjunction with Levenberg–Marquardt non-linear least-square fit (LM-fit) and line-broadening analysis, demonstrates that this approach is indeed the case for nanocrystalline Al alloys that have been subjected to severe plastic deformation. The estimation of the lattice microstrain of LiH was not feasible in this study because its high angle reflections disappeared after ball milling.

Fourier transform infrared (FTIR) analysis (Nicolet, Magna-IR 560) was conducted on the hydrogenated samples in order to check if $LiBH_4$ was generated during hydrogenation. Around 1 wt.% hydrogenated powder was mixed and ground with KBr powder in a glovebox filled with Ar of 99.999% purity. The ground mixture was subsequently pressed into a pellet 1 cm in diameter in air very

quickly (~30 s) in order to avoid excessive oxidization. Although the hydride powder on the pellet surface was oxidized, the hydride powder in the interior was not because of the protection from 99 wt.% KBr powder in the mixture. Prior to the collection of each spectrum, the background of air was measured and subtracted from the sample.

Powders under various conditions were also characterized for their specific surface areas (SSA) through nitrogen adsorption at 77 K based on the Brunauer–Emmett–Teller (BET) method [41] using a gas sorption analyzer (NOVA 1000, QUANTACHROME Corporation, FL). The loading of the sample (~0.05 g) into a sample cell with a Teflon stem filler was performed in a glovebox filled with Ar of 99.999% purity. The measurement was performed immediately after the sample was loaded in the instrument. The relative pressure (P/P_0) was 0.05–0.3 and the reported SSA data were calculated based on 5 points BET method.

3. Results and discussion

Fig. 1 shows the effect of ball milling duration on hydriding and dehydriding behavior of $2LiH + MgB_2$ mixtures ball milled with no additive. An increase in overall storage capacity and a lowering of the onset temperature for hydrogen uptake are witnessed as the ball milling duration is increased. Specifically, the mixture ball milled for 120 h shows a total capacity of 8.3 wt.% H_2 with significant uptake beginning at ~150 °C, while the 24- and 3-h ball milled samples only store 5.5 wt.% and 3.2 wt.% H_2 with significant uptake beginning at ~175 °C and ~200 °C, respectively. The dehydriding attributes of the $2LiH + MgB_2$ mixture are also dependent on the ball milling duration. The 120-h ball milled mixture is able to release 2.0 wt.% H_2 with significant liberation beginning at ~240 °C, while the same mixture ball milled for only 24 h exhibits total release of only 1.5 wt.% H_2 with the onset of significant liberation beginning at ~250 °C. These results unambiguously reveal that a longer ball milling duration results in enhanced hydriding and dehydriding performance of $2LiH + MgB_2$ mixtures.

The addition of Mn and V to the $2LiH + MgB_2$ system has varying effects on the hydriding and dehydriding properties of ball milled mixtures. The effect of V is divulged in Fig. 2. Note that the hydrogenation behaviors of $2LiH + MgB_2$ mixtures with and without V addition are very similar. For the 24-h ball milled mixtures with and without V, both the onset temperatures and the total amounts of hydrogen uptake are almost identical. For the 120-h ball milled mixtures, the onset temperatures for hydrogen uptake are nearly the same; but the total amount of hydrogen absorbed by the mixture with V is slightly lower than the counterpart without V, exhibiting a ~4.8% decrease. Thus, the addition of V has little or no effect on the hydrogenation behavior of the $2LiH + MgB_2$ system. In contrast, the dehydrogenation behavior of the $2LiH + MgB_2$ system has been improved substantially by the addition of V. As shown in Fig. 2, the total amount of hydrogen released from the $2LiH + MgB_2 + 0.05V$ mixture ball milled for 120 h is 3.3 wt.%, representing a 65% increase over that released by the $2LiH + MgB_2$ mixture. Similarly, the mixture with V ball milled for 24 h displays a 42% improvement in the hydrogen released over the counterpart without V.

Interestingly, the effect of Mn is very different from that observed for V. Fig. 3 compares the hydrogenation and dehydrogenation behavior of $2LiH + MgB_2$ mixtures with and without Mn and V dopants. Note that the hydrogen uptake rate for the

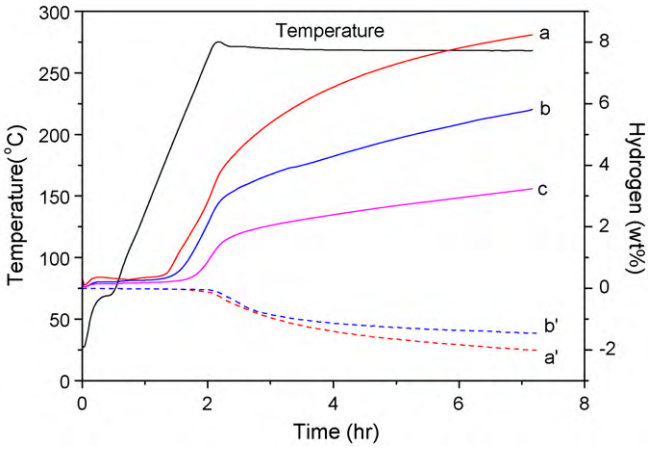

Fig. 1. Hydriding (solid line) and dehydriding (dotted line) curves of $2LiH + MgB_2$ mixtures ball milled for (a) and (a′) 120 h, (b) and (b′) 24 h, and (c) 3 h. The temperature ramp as a function of time is the same for both hydriding and dehydriding experiments. Hydriding is conducted under a H_2 pressure of 90 bar, whereas dehydriding is performed under a H_2 pressure of ~0.01 bar.

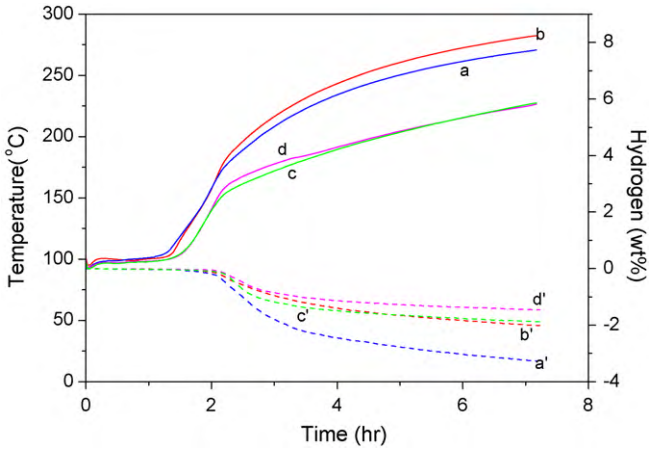

Fig. 2. Comparisons of hydriding and dehydriding behaviors of ball-milled $2LiH + MgB_2$ and $2LiH + MgB_2 + 0.05V$ mixtures. The hydriding and dehydriding conditions are identical to those shown in Fig. 1. Keys: (a) hydriding and (a′) dehydriding curve of the 120 h ball-milled $2LiH + MgB_2 + 0.05V$ mixture, (b) hydriding and (b′) dehydriding curve of the 120 h ball-milled $2LiH + MgB_2$ mixture, (c) hydriding and (c′) dehydriding curve of the 24 h ball-milled $2LiH + MgB_2 + 0.05V$ mixture, and (d) hydriding and (d′) dehydriding curve of the 24 h ball-milled $2LiH + MgB_2$ mixture. All the dehydriding experiments are conducted after the hydriding experiments shown here.

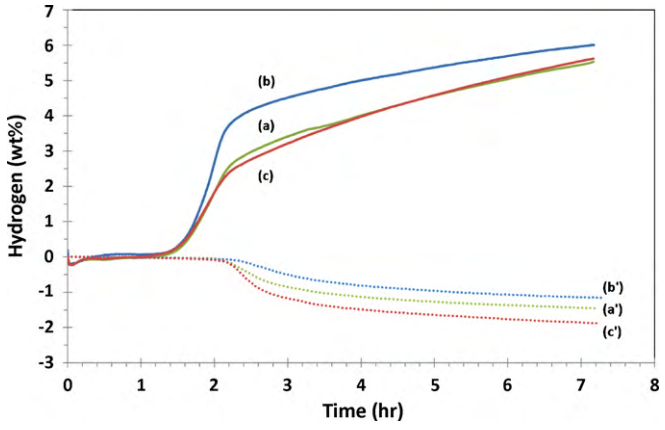

Fig. 3. Hydrogenation and dehydrogenation behaviors of 24 h ball-milled $2LiH + MgB_2$ mixtures with and without dopants. The hydriding and dehydriding conditions are identical to those shown in Fig. 1. Keys: (a) hydriding and (a′) dehydriding curve of $2LiH + MgB_2$, (b) hydriding and (b′) dehydriding curve of $2LiH + MgB_2 + 0.05Mn$, and (c) hydriding and (c′) dehydriding curve of $2LiH + MgB_2 + 0.05V$. All the dehydriding experiments are conducted after the hydriding experiments shown here.

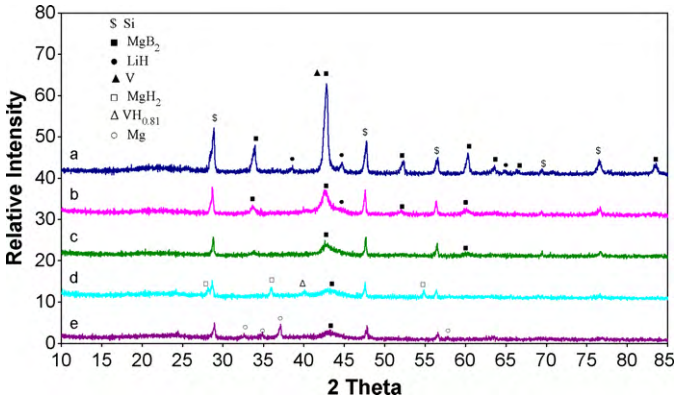

Fig. 4. X-ray diffraction patterns from 2LiH + MgB_2 + 0.05V mixtures before and after ball milling, hydrogenation and dehydrogenation: (a) without ball-milling, (b) after 24 h ball-milling, (c) after 120 h ball-milling, (d) after 120 h ball-milling and then hydrogenation, and (e) after 120 h ball-milling, then hydrogenation, and finally dehydrogenation. The hydrogenation and dehydrogenation conditions are shown in Fig. 2.

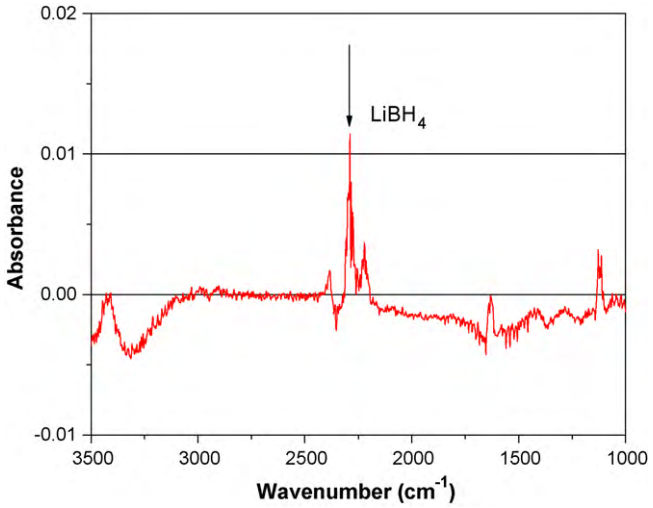

Fig. 5. The FTIR pattern of the 120 h ball-milled 2LiH + MgB_2 + 0.05V mixture after hydrogenation.

2LiH + MgB_2 + 0.05Mn mixture at the temperature range between 190 and 250 °C (i.e., between 1.5 and 2.5 h in terms of time) is substantially higher than that of the mixtures with and without the V dopant. As a result, the total amount of hydrogen absorbed after a 5 h holding at 265 °C under a 90 bar hydrogen pressure is higher for the 2LiH + MgB_2 + 0.05Mn mixture, as compared to the mixtures with and without V. Thus, Mn has clearly enhanced the hydrogenation process at temperatures ranging from 190 to 250 °C. In contrast, the dehydrogenation behavior of the 2LiH + MgB_2 mixture with Mn is slightly inferior to both mixtures with and without V. Based on these results, it can be concluded that the Mn dopant provides the best enhancement in hydrogenation, while the V dopant offers the best improvement in dehydrogenation.

To understand these phenomena, detailed XRD studies have been conducted. Fig. 4 shows the evolution of the XRD pattern of the 2LiH + MgB_2 + 0.05V mixture under various conditions. Several interesting phenomena are noted from these XRD patterns. First, XRD spectra of 0-, 24- and 120-h ball milled mixtures contain the peaks of LiH and MgB_2 clearly. Further, the peak intensities of LiH and MgB_2 decrease with increasing the ball milling duration, indicating the introduction of structural defects into crystalline LiH and MgB_2. In contrast, the peaks of V are not obvious in the spectra because (i) the small amount of V added to the mixture is around the detection level of the X-ray instrument and (ii) the strongest peak of V at 42.171° partially overlaps with the peak of MgB_2 at 42.4346°. Second, the spectra indicate no new phases formed in the ball-milled state, suggesting little or no chemical reactions during ball milling. Third, shifting of MgB_2 peaks are present. For example, the strongest peak from the combined MgB_2 (1 0 1) and V (1 1 0) peaks at 42.418° has down shifted by 0.0183° after ball milling for 24 h. This strongest peak, however, is up shifted by 0.0725° after ball milling for 120 h. Details of this peak position as a function of the ball milling condition are summarized in Table 1. Fourth, by comparing XRD spectra (a), (b) and (c), it is clear that high-energy ball milling has broadened XRD peaks of all the chemicals in the system, including MgB_2, LiH, and the contaminant LiOH from the as-purchased LiH powder. Fifth, peaks corresponding to MgH_2 and $VH_{0.81}$ appear in the hydrogenated sample (XRD spectrum (d)). Here, the strongest peak of $VH_{0.81}$, not VH, appears at 39.83°. However, no $LiBH_4$ peaks can be found, which is similar to the case of the ball milled 2LiH + MgB_2 system [29]. Finally, the intensities of both MgH_2 and $VH_{0.81}$ reflections disappear after dehydrogenation, accompanied by the appearance of Mg peaks.

To confirm the formation of $LiBH_4$ from the hydrogenation reaction, FTIR analysis was conducted. As shown in Fig. 5, the characteristic absorption frequencies of the $[BH_4]^-$ complex appear at 2385, 2289, 2223 and 1124 cm^{-1} in the FTIR spectrum of the powder mixture after hydrogenation. Therefore, combining results of XRD and FTIR, it can be concluded that MgH_2 and $LiBH_4$ are formed in the hydrogenation process with the co-formation of $VH_{0.81}$. Thus, the hydriding reaction may be summarized as below:

$$2LiH + MgB_2 + 0.05V + 4.02025H_2 \Leftrightarrow 2LiBH_4 + MgH_2 + 0.05VH_{0.81} \quad (4)$$

Note that the partial or complete dissolution of V into MgB_2 induced by ball milling is not reflected in the equation above, but will be discussed later.

Detailed XRD studies have also been conducted for the 2LiH + MgB_2 + 0.05Mn mixture under various conditions. As shown

Table 1
Shifting of the MgB_2 (1 0 1) diffraction peak as a function of the dopant and ball milling duration[a].

Sample ID	Ball milling condition (h)	Si (2 2 0) peak (2θ, degree)	MgB_2 (1 0 1) peak (2θ, degree)	Shifting of MgB_2 (1 0 1) peak (2θ, degree)
2LiH + MgB_2	0	47.3400	42.4346[b]	0
2LiH + MgB_2	120	47.3400	42.4111	−0.0235
2LiH + MgB_2 + 0.05Mn	0	47.3400	42.4387[b]	0
2LiH + MgB_2 + 0.05Mn	3	47.3400	42.4603	0.0216
2LiH + MgB_2 + 0.05Mn	24	47.3400	42.5315	0.0928
2LiH + MgB_2 + 0.05V	0	47.3400	42.4180[b]	0
2LiH + MgB_2 + 0.05V	24	47.3400	42.3997	−0.0183
2LiH + MgB_2 + 0.05V	120	47.3400	42.4905	0.0725

[a] All the XRD patterns were calibrated with the Si (2 2 0) peak based on the PDF card of Si (27-1402).
[b] Note that the MgB_2 (1 0 1) peak at 42.4346° is partially overlapped with the Mn (3 3 0) peak at 43.016° in the Mn-containing system and with the V (1 1 0) peak at 42.171° in the V-containing system. As a result, the positions of the so-called MgB_2 (1 0 1) peaks before ball milling are slightly different.

Table 2
Crystallite sizes and lattice microstrains derived from XRD peak broadening.

Sample ID	Ball milling time (h)	MgB_2 crystallite size (nm)	LiH crystallite size (nm)	MgB_2 lattice microstrain
$2LiH + MgB_2 + 0.05Mn$	0	74.5	>100	0.0022
$2LiH + MgB_2 + 0.05Mn$	3	28.7	31.7	0.0042
$2LiH + MgB_2 + 0.05Mn$	24	15.5	42.5315	0.0134
$2LiH + MgB_2 + 0.05V$	0	86.5	>100	0.0021
$2LiH + MgB_2 + 0.05V$	24	35.5	27.2	0.0050
$2LiH + MgB_2 + 0.05V$	120	30.8	23.6	0.0059

in Fig. 6, the key features of peak broadening and shifting observed in the V-containing system are also present in the Mn-containing system. However, the detail of peak shifting for the Mn-containing system is different from the V-containing system. As summarized in Table 1, 120 h ball milling of $2LiH + MgB_2$ without dopants has down shifted the MgB_2 (1 0 1) peak from 42.4346° before ball milling to 42.4111° (i.e., 2θ is decreased by 0.0235° which is well beyond the error range of the analysis). Peak shifting is an indication of the formation of a MgB_2-based solid solution, which supports the previous NMR analysis that indicates the formation of the ternary compound $(Mg_{1-x}Li_{2x})B_2$, resulting from ball milling of the $2LiH + MgB_2$ mixture [30–32]. Adding the Mn dopant, however, has led to up-shifting of the MgB_2 (1 0 1) peak, indicating a contraction of the MgB_2 (1 0 1) planar spacing and suggesting the dissolution of Mn into the ternary compound $(Mg_{1-x}Li_{2x})B_2$, with an effect on the MgB_2 (1 0 1) planar spacing opposite to that of Li. This Mn effect becomes stronger as the ball milling duration increases.

The effect of V on the peak shifting is smaller than that of Mn, but is also opposite to that of Li. As shown in Table 1, with 24 h of ball milling the addition of Mn has resulted in the up-shifting of the MgB_2 (1 0 1) peak by 0.0928°. This value is approached by the V-containing system only after 120 h of ball milling (i.e., 0.0725° up-shifting). Note that the net peak shifting induced by V with 120 h of ball milling should be taken as 0.096°, that is, shifting the 2θ value (42.4111°) of the ternary compound $(Mg_{1-x}Li_{2x})B_2$ with 120 h of ball milling to the 2θ value (42.4905°) of the ternary compound $(Mg_{1-x}Li_{2x})B_2$ containing the V dopant. For the case of 24 h of ball milling, the effect of V is very small or not present because the MgB_2 (1 0 1) peak is still down shifted by 0.0183°, suggesting that the shifting at this stage is still dominated by Li. Thus, it can be concluded that the dissolution of both Mn and V into MgB_2 result in a contraction of the MgB_2 (1 0 1) planar spacing, but Mn has a stronger effect than V. These phenomena may result from the possibility that Mn is easier to dissolve into MgB_2 than V or the possibility that V results in less distortion of the MgB_2 lattice. The latter has been predicted by the first-principles calculation [35]. However, the present study cannot distinguish one mechanism from the other.

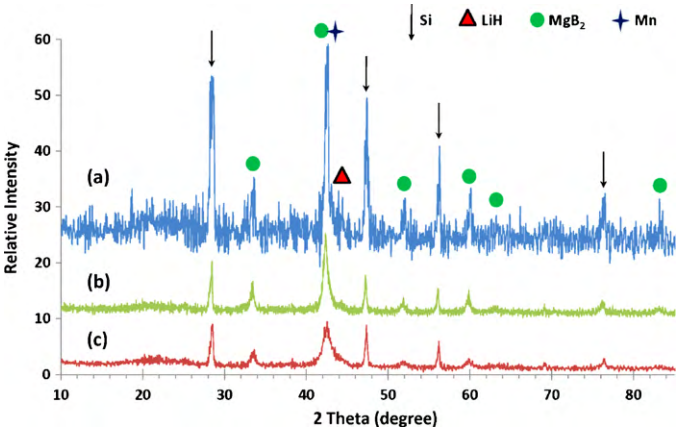

Fig. 6. X-ray diffraction patterns from $2LiH + MgB_2 + 0.05Mn$ mixtures before and after ball milling: (a) without ball milling, (b) after 3 h ball milling, and (c) after 24 h ball milling.

Other powder characteristics (e.g., the crystallite size, lattice microstrain, and SSA) do not alter substantially with the addition of Mn and V. As shown in Table 2, both Mn- and V-containing systems exhibit the same trend of a decrease in the crystallite size and an increase in the lattice microstrain with increasing the ball milling duration. Furthermore, both systems show similar values of the crystallite sizes, suggesting that Mn and V dopants have little or no effect on the crystallite sizes of LiH and MgB_2. However, the lattice microstrain is clearly higher in the Mn-containing system than in the V-containing system. This phenomenon is consistent with the stronger effect of Mn than V in the peak shifting and lattice distortion discussed above. The SSA measurements reveal little difference in the two systems because the SSA of the powder mixture has been reduced from 4.06 $m^2\,g^{-1}$ before milling to 10.94 and 10.14 $m^2\,g^{-1}$ for the Mn- and V-containing systems, respectively.

Taking together all of the data analyzed above, we can argue that the enhancement of Mn in the hydrogenation process is due to its strong effect on the lattice distortion, thereby increasing the Mg diffusion coefficient in the $(Mg_{1-x}Li_{2x})B_2$ compound, which in turn increases the H_2 absorption kinetics. In contrast, V has little impact on the hydriding behavior because of its low intrinsic capability to induce the lattice distortion and thus to enhance Mg diffusion, as predicted by the first-principles calculation [35]. However, V exhibits clear advantages in enhancing the dehydrogenation process because of the formation of $VH_{0.81}$ during hydriding. This $VH_{0.81}$ decomposes before MgH_2 during the dehydriding process and thus it behaves like a "hydrogen pump" to increase the rate of MgH_2 decomposition. This phenomenon is in good accordance with other studies [42–45] showing that addition of V can increase the rate of MgH_2 decomposition. The increase in MgH_2 decomposition, in turn, results in the increase in Mg available to induce the decomposition of $LiBH_4$, as proposed by several previous studies [7,8,29].

4. Conclusions

The effects of Mn and V dopants on the hydriding and dehydriding properties of the $2LiH + MgB_2$ system have been investigated. It is found that Mn addition promotes the lattice distortion of MgB_2 crystals and thus enhances the diffusion of Mg vacancies within MgB_2, which in turn increases the hydrogenation kinetics of the $2LiH + MgB_2$ system. In contrast, V addition does not result in an increase in the hydrogenation kinetics because of its lower capacity in producing the lattice distortion of MgB_2 crystals. However, V addition leads to the enhanced dehydrogenation kinetics because of the formation of $VH_{0.81}$ during hydrogenation. This $VH_{0.81}$ behaves like a "hydrogen pump" to increase the rate of MgH_2 decomposition and thus the dehydrogenation kinetics.

Acknowledgements

This work was supported under the U.S. Department of Energy (DOE) Contract No. DE-FC36-05GO15008. The vision and support of

Drs. Carole J. Read and Ned T. Stetson, DOE Technology Managers, are greatly appreciated.

References

[1] L. Schlapbach, A. Zuttel, Nature 414 (2001) 353–358.
[2] J. Soulie, G. Renaudin, R. Cerny, K. Yvon, J. Alloys Compd. 346 (2002) 200–205.
[3] A. Zuttel, P. Wenger, S. Rentsch, P. Sudan, Ph. Mauron, Ch. Emmenegger, J. Power Sources 118 (2003) 1–7.
[4] A. Zuttel, S. Rentsch, P. Fischer, P. Wenger, P. Sudan, Ph. Mauron, Ch. Emmenegger, J. Alloys Compd. 356–357 (2003) 515–520.
[5] G.P. Meisner, M.L. Scullin, M.P. Balogh, F.E. Pinkerton, M.S. Meyer, J. Phys. Chem. B 110 (2006) 4186–4192.
[6] J.J. Vajo, T.T. Salguero, A.F. Gross, S.L. Skeith, G.L. Olson, J. Alloys Compd. 446–447 (2007) 409–414.
[7] J.J. Vajo, S.L. Skeith, F. Mertens, J. Phys. Chem. B 109 (2005) 3719–3722.
[8] X.B. Yu, D.M. Grant, G.S. Walker, Chem. Commun. (2006) 3906–3908.
[9] J. Kostka, W. Lohstroh, M. Fichtner, H. Hahn, J. Phys. Chem. C 111 (2007) 14026–14029.
[10] J.J. Vajo, G.L. Olson, Scr. Mater. 56 (2007) 829–834.
[11] A.F. Gross, J.J. Vajo, S.L. Van Atta, G.L. Olson, J. Phys. Chem. C 112 (2008) 5651–5657.
[12] X.B. Yu, Z. Wu, Q.R. Chen, Z.L. Li, B.C. Weng, T.S. Huang, Appl. Phys. Lett. 90 (2007) 034106.
[13] Y. Zhang, W.-S. Zhang, A.-Q. Wang, L.-X. Sun, M.-Q. Fan, H.-L. Chu, J.-C. Sun, T. Zhang, Int. J. Hydrogen Energy 32 (2007) 3976–3980.
[14] A. Zuttel, A. Borgschulte, S.-i. Orimo, Scr. Mater. 56 (2007) 823–828.
[15] Y. Nakamori, S.-i. Orimo, J. Alloys Compd. 370 (2004) 271–275.
[16] K. Miwa, N. Ohba, S.-i. Towata, Y. Nakamori, S.-i. Orimo, Phys. Rev. B 69 (2004) 245120.
[17] S. Orimo, Y. Nakamori, A. Zuttel, Mater. Sci. Eng. B 108 (2004) 51–53.
[18] K. Miwa, N. Ohba, S.-i. Towata, Y. Nakamori, S.-i. Orimo, J. Alloys Compd. 404–406 (2005) 140–143.
[19] Y. Nakamori, K. Miwa, A. Ninomiya, H. Li, N. Ohba, S.-i. Towata, A. Zuttel, S.-i. Orimo, Phys. Rev. B 74 (2006) 045126.
[20] S.-i. Orimo, Y. Nakamori, G. Kitahara, K. Miwa, N. Ohba, S.-i. Towata, A. Zuttel, J. Alloys Compd. 404–406 (2005) 427–430.
[21] J.J. Vajo, S.L. Skeith, F. Mertens, S.W. Jorgensen, J. Alloys Compd. 390 (2005) 55–61.
[22] Y. Nakamori, A. Ninomiya, G. Kitahara, M. Aoki, T. Noritake, K. Miwa, Y. Kojima, S.-i. Orimo, J. Power Sources 155 (2006) 447–455.
[23] M. Au, A. Jurgensen, J. Phys. Chem. B 110 (2006) 7062–7067.
[24] M. Au, A. Jurgensen, K. Zeigler, J. Phys. Chem. B 110 (2006) 26482–26487.
[25] J. Yang, A. Sudik, C. Wolverton, J. Phys. Chem. C 111 (2007) 19134–19140.
[26] F.E. Pinkerton, M.S. Meyer, G.P. Meisner, M.P. Balogh, J.J. Vajo, J. Phys. Chem. C 111 (2007) 12881–12885.
[27] T. Nakagawa, T. Ichikawa, N. Hanada, Y. Kojima, H. Fujii, J. Alloys Compd. 446–447 (2007) 306–309.
[28] D.J. Siegel, C. Wolverton, V. Ozolins, Phys. Rev. B 76 (2007) 134102.
[29] X. Wan, T. Markmaitree, W. Osborn, L. Shaw, J. Phys. Chem. C 112 (2008) 18232–18243.
[30] J.-Z. Hu, J.-H. Kwak, Z.-G. Yang, X. Wan, L. Shaw, Appl. Phys. Lett. 94 (2009) 141905.
[31] J.-Z. Hu, J.-H. Kwak, Z. Yang, X. Wan, L. Shaw, J. Power Sources 195 (2010) 3645–3648.
[32] L. Shaw, X. Wan, J.Z. Hu, J.H. Kwak, Z. Yang, J. Phys. Chem. C 114 (2010) 8089–8098.
[33] I. Barin, O. Knacke, Thermochemical Properties of Inorganic Substances, Springer-Verlag, Berlin, 1973.
[34] T.B. Massalski (Ed.), Binary Alloy Phase Diagrams, ASM International, Materials Park, OH, USA, 1986.
[35] Y. Zhong, H. Zhu, L. Shaw, R. Ramprasad, unpublished research.
[36] Z.-G. Yang, L. Shaw, Nanostruct. Mater. 7 (1996) 873–886.
[37] H.P. Klug, L.E. Alexander, X-ray Diffraction Procedures for Polycrystalline and Amorphous Materials, John Wiley & Sons, Inc., New York, NY, 1974.
[38] A.R. Stokes, A.J.C. Wilson, Proc. Phys. Soc. London 56 (1944) 174–181.
[39] L. Shaw, J. Villegas, H. Luo, D. Miracle, Acta Mater. 51 (2003) 2647–2663.
[40] A.L. Ortiz, L. Shaw, Acta Mater. 52 (2004) 2185–2197.
[41] S. Brunauer, P.H. Emmett, E. Teller, J. Am. Chem. Soc. 60 (1938) 309–319.
[42] G. Liang, J. Huot, S. Boily, A. Van Neste, R. Schulz, J. Alloys Compd. 291 (1999) 295–299.
[43] G. Liang, J. Huot, S. Boily, A. Van Neste, R. Schulz, J. Alloys Compd. 292 (1999) 247–252.
[44] H. Reule, M. Hirscher, A. Weiβhardt, H. Kronmuller, J. Alloys Compd. 305 (2000) 247–252.
[45] G. Liang, S. Boily, J. Huot, A. Van Neste, R. Schulz, J. Alloys Compd. 268 (1998) 302–307.